Science of the Total Environment 894 (2023) 165017

Contents lists available at ScienceDirect

Science of the Total Environment

journal homepage: www.elsevier.com/locate/scitotenv

Role of the active chlorine generated in situ on the photoelectrocatalytic inactivation of bacteria and fungi with TiO_2 nanotubes

Cristina Adán, Cristina Pablos, Patricia Misis, Sandra Pascua, Javier Marugán *

Chemical and Environmental Engineering Group. ESCET, Universidad Rey Juan Carlos. c/Tulipán s/n 28933 Móstoles, Spain

HIGHLIGHTS

- *E. coli* inactivation is higher as the chlorine formation increases in PEC.
- Chlorine increases as nanotubes length and applied potential bias increases.
- Higher Cl^- ion concentration improves the inactivation of *E. coli*.
- NaCl electrolyte is more effective than $CaCl_2$ in the inactivation of *E. coli*.
- The inactivation of *E. coli* is higher than *E. faecalis* and *C. albicans*.

GRAPHICAL ABSTRACT

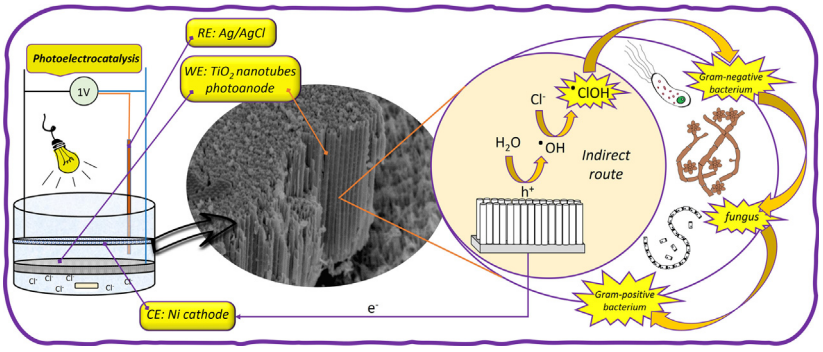

ARTICLE INFO

Editor: Damià Barceló

Keywords:
TiO_2 nanotubes
Photoelectrocatalysis
Microorganisms' inactivation
Chloride electrolytes
Active chlorine

ABSTRACT

Immobilised TiO_2 nanotube (TiO_2-NT) electrodes were grown via electrochemical anodisation in an aqueous solution containing fluoride ions at 10, 20 and 30 V. The photocatalytic (PC) and photoelectrocatalytic (PEC) activity of TiO_2-NTs electrodes in the oxidation of methanol and the inactivation of bacteria and fungi was studied in different chloride salts electrolytes. Low concentrations of electrochemically generated oxidising species, such as free chlorine, were measured in experiments at pH 8.5 and +1 V of applied potential. Increasing the anodising potential results in longer nanotubes with higher photoactivity. The TiO_2-NT electrode anodised at 30 V (TiO_2-NT30V) generates free chlorine with an average concentration of 0.03 $mg{\cdot}L^{-1}$ upon illumination with UV-A at +1 V of potential bias. This concentration was enough to achieve 99.99 % of inactivation of a 10^6 $CFU{\cdot}mL^{-1}$ Gram-negative bacteria (*Escherichia coli*) in <3 min and Gram-positive bacteria (*Enterococcus faecalis*) after 7 min, whereas fungi (*Candida albicans*) required 15 min. The low production of chlorine was found to have a big impact on the bacteria and fungi inactivation even in not favourable chlorine generation conditions. An in situ investigation of the most influential parameters in the inactivation of some microorganisms with PEC and NT30V electrode has been done. It was found that free chlorine production increases with the length of TiO_2-NT, with Cl^- concentration up to 15 $mmol{\cdot}L^{-1}$ and with the application of potential bias. TiO_2-NT30V photoanode has been demonstrated to produce active chlorine at levels compatible with the water disinfection process, suggesting that the present method could be considered a promising alternative for in situ chlorine-based disinfection.

1. Introduction

Electrochemical production of active chlorine is a well-known process for water decontamination and disinfection (Sirés et al., 2014; Brillas and Martínez-Huitle, 2015; Huang et al., 2016; Scialdone et al., 2021; Sales Monteiro et al., 2021). Electrochemical chlorine generation brings the

* Corresponding author.
E-mail address: javier.marugan@urjc.es (J. Marugán).

http://dx.doi.org/10.1016/j.scitotenv.2023.165017
Received 12 April 2023; Received in revised form 31 May 2023; Accepted 18 June 2023
Available online 21 June 2023

possibility to eliminate the old production chlorine methods and eliminate the storage and handling of hazardous chlorine gas or corrosive acid solutions (Kraft et al., 1999; Chung et al., 2018). Recent research has shown that catalysts based on dimensionally stable anodes (DSA®), such as RuO_2/Ti, IrO_2/Ti, SnO_2/Ti and Ta_2O_5/Ti and TiO_2/Ti-based electrodes can be used in the electrochemical production of chlorine with very favourable yields to avoid the oxygen evolution reaction (OER) that competes with the formation of chlorine and reduce cost-effective anodic materials (Oliveira et al., 2007; Jeong et al., 2009; Le Luu et al., 2015; Kim et al., 2018; Scialdone et al., 2021). Since TiO_2 is also a photocatalytic material, it has been used in the photoelectrochemical production of chlorine in recent years (Zanoni et al., 2004; Selcuk and Anderson, 2005; Cheng et al., 2007; Fraga et al., 2009; Li et al., 2013; Xiao et al., 2016; Zhao et al., 2019; Mesones et al., 2020; García-Espinoza et al., 2021). The study of TiO_2 photoanode employs a wide variety of configurations, such as RuO_2-TiO_2/Ti (Zhao et al., 2019), Ti/TiO_2 thin-film (Zanoni et al., 2004; Cheng et al., 2007; Fraga et al., 2009), nanoporous TiO_2 (Selcuk and Anderson, 2005), TiO_2/ITO photoanodes (Li et al., 2013), TiO_2 nanotubes arrays (Xiao et al., 2016) or even GA-TiO_2 composites used as bipolar electrodes (Mesones et al., 2020) that have been used to generate active chlorine by the photoelectrocatalytic way under UVA light illumination under favourable conditions. However, special attention must be paid since, during the photoelectrocatalytic process in aqueous conditions, active chlorine can be generated in a very low or even undetectable concentration which, in some cases, may cause overestimation of photoanode activity. The generation of chlorine in the photoelectrocatalytic processes is conditioned by several factors that depend on: i) the type of electrodes employed, and ii) the reaction conditions. Accordingly, these two factors condition the mechanism for the formation of active chlorine species.

The parameters that affect the photoelectrocatalytic production of chlorine with TiO_2-based electrodes have been already reported, including the type of TiO_2 electrode material, pH solution, electrolyte Cl^- concentration, applied potential bias or current density, competition with other ions and time (Zanoni et al., 2004; Selcuk and Anderson, 2005; Cheng et al., 2007; Fraga et al., 2009). Among them, the parameters that most affect chlorine production are the pH of the solution and the concentration of chloride ions. Several authors have reported that chlorine production is favoured by acid pH, being the best conditions around pH 2–4 (Zanoni et al., 2004; Selcuk and Anderson, 2005; Cheng et al., 2007; Fraga et al., 2009). Maintaining pH constant during the experiments, photoelectrocatalytic chlorine production with TiO_2 photoelectrodes is much higher under acidic conditions (pH < 6), while at pH values higher than 6, the active chlorine generation decreases sharply, and the process is completely suppressed at pH > 11.

The photoelectrocatalytic production of active chlorine as a function of the concentration of chloride ions (0.5 mmol·L^{-1} to 250 mmol·L^{-1} of Cl^-) has also been investigated at pH 4.0 and an applied potential of +1 V (Zanoni et al., 2004; Cheng et al., 2007). At acid pH, higher active chlorine production is obtained by an increase in chloride ion concentration. Nevertheless, further increasing the chloride concentration above 100 mmol·L^{-1} does not promote any improvement, thereby showing a limiting rate in the oxidation of chloride ions. These results indicate that the area of the electrode at a higher concentration limits the active chlorine production rate. In the same way, the same experiments performed applying a current density of 30 mA·cm^{-2} have shown similar results (Zhao et al., 2019).

The study of different potential bias (between −0.4 V and +1 V) applied for the photoelectrocatalytic generation of active chlorine with TiO_2 electrodes in a chloride concentration of 25 mmol·L^{-1} at pH 4 were also reported (Zanoni et al., 2004; Selcuk and Anderson, 2005). The results of this investigation indicate that chlorine generation is zero when the applied potential is −0.4 V, while at potentials between −0.2 V and +0.4 V, there is a linear increase in active chlorine production rate, which appears to be constant at higher applied potentials and indicates that maximum chloride conversion has been obtained since the maximum charge separation has also been attained (Zanoni et al., 2004). In the case of the application of a current density instead of a potential bias, the results differ (Zanoni et al., 2004). Under fixed initial chloride concentration of 100 mmol·L^{-1}, pH 4 and UVA irradiation, there is a significant increase in chlorine production from 5 to 30 mA·cm^{-2}, while for higher current density at 50 mA·cm^{-2}, there is a slight decrease in the chlorine production. These results indicate that applied current density improves the photoelectrochemical process due to the minimisation of charge carriers (e^-/h^+) recombination up to 30 mA·cm^{-2}, while at higher current density, the process could be limited by mass transport conditions and/or chlorate production as a parallel reaction occurring at the photoanode (Zhao et al., 2019).

Taking into account the knowledge extracted from the scientific literature, the best conditions for the PEC production of free chlorine in TiO_2-based photoanodes are electrolytes with Cl^- concentration of 0.05 mol·L^{-1} at pH around 2.0–4.0 and with an application of potential bias higher than +0.4 V (Zanoni et al., 2004; Selcuk and Anderson, 2005; Cheng et al., 2007; Fraga et al., 2009) or with a current density of 30 mA·cm^{-2} (Zhao et al., 2019).

However, there are still few studies that have monitored the in situ generation of active chlorine species during the PEC degradation of pollutants with TiO_2-based electrodes (Selcuk and Anderson, 2005; Cheng et al., 2007; Fraga et al., 2009; Zhao et al., 2019; Xiao et al., 2016; Xiao et al., 2019), and only the work of Li et al., (Li et al., 2013) has reported the possibility to use in situ photoelectrogenerated active chlorine to improve microorganisms inactivation in real conditions for water disinfection. These authors have reported the bactericidal performances of photocatalytic and photoelectrocatalytic systems in the absence and presence of low concentrations of Cl^- and Br^- (Li et al., 2011)(Li et al., 2013). PEC (with a +0.3 V applied potential bias) and an initial concentration of 9.0×10^6 CFU·mL^{-1} *E. coli* confirmed that PEC–Cl inactivation efficiency in the presence of 1.0 mmol·L^{-1} Cl^- requires only 23.3 s to achieve total inactivation, 13 times faster than that of the PEC method in the absence of Cl^-.

The application of an external anodic potential in chloride electrolytes is prone to form chlorine that modifies the expected results in the photoelectrocatalytic process even with basic pHs. This fact must be considered when measuring the photoelectrocatalytic activity of TiO_2-based electrodes. To carry out a good evaluation of the PEC process, trapping agents must be used to block the production of chlorinated by-products or perform the pertinent chlorine measurements in order to correctly evaluate the contribution of each process. This work reports the photoelectrocatalytic inactivation of several microorganisms with the in situ generation of low concentrations of free chlorine by using titanium dioxide nanotubes (TiO_2-NT) and studying the different parameters that have the most influence on the generation of chlorine. The study has demonstrated that low chlorine concentrations can be formed in unfavourable conditions, which is enough to inactivate bacterial and fungus concentrations of 10^6 CFU·mL^{-1} in <15 min.

2. Materials and methods

2.1. Preparation of TiO_2-NTs photoelectrodes

Commercial titanium sheets (99.6 % purity) of 5 cm in diameter and 0.5 mm thickness were supplied Goodfellow Inc. Before anodisation, the sheets were degreased through sonication in ethanol for 15 min and rinsed with deionised water several times. Then the foils were immersed again for two minutes in an $HF/HNO_3/H_2O$ (1:4:5 v/v) solution and rinsed again in abundant deionised water. After the cleaning procedure, two titanium wires were spot-welded to each of the sheets to provide electrical contact for the anodisation process and the photoelectrocatalytic reactions.

The anodisation process was conducted in a two-electrode electrochemical cell connected to a DC power supply (ISO-TECH, model IPS 303DD). A nickel mesh (Goodfellow Inc., 55 % open area) was used as the cathode at a distance of 1 cm from the titanium photoanode. Subsequently, the electrolytic solution was added to the electrochemical cell, and then the selected anodisation potential was applied without magnetic stirring. Three electrodes were anodised with an electrolyte composed of ethylene glycol,

water 5 wt% and NH_4F (0.15 mol·L^{-1}). The electrodes were anodised keeping the applied potential constant at 10, 20 and 30 V for 120 min without agitation and were named TiO_2-NT10V, TiO_2-NT20V and TiO_2-NT30V. After the anodisation process, the titanium foils were cleaned with abundant water and dried at 100 °C for 24 h. Afterwards, the electrodes were annealed at 450 °C for two hours with a heating rate of 2 °C/min to induce anatase crystallisation.

2.2. Physico-chemical characterisation of the TiO_2-NTs electrodes

To determine the calcination treatment of the electrodes, the temperature chamber of the Philips X'PERT MPD diffractometer with an XCell detector using a Cu Kα monochromatic radiation was employed. The diffractograms were recorder at 10 °C/min up to 100 °C and 2 °C/min up to 600 °C at a scanning speed of 0.01°/s with an accumulation time of 2 s per point.

Raman spectra were obtained with a HORIBA Jovin-Yvon spectrometer model HR800UV equipped with an Olympus BX41 optic microscope. TiO_2-NTs electrodes were excited with a red laser of 632.8 nm and spectra were registered between 100 and 800 cm^{-1}.

Morphology, length, diameter and wall thickness of the nanotubes were evaluated using high-resolution Scanning Electron Microscopy (SEM). The images were taken on a Nova Nano SEM230 (FEG-SEM) microscope working with acceleration voltages between 2 and 10 kV and equipped with ETD, TLD, BSD, Helix, and CD detectors. Samples were previously prepared by scratching the intact surface of the electrode and rotating the sample holder 45° to obtain the length of the TiO_2-NTs. The *Digital Micrograph 365 Demo* program from Gatan Software Company helped to analyse SEM images. The average of pore diameter, wall thickness and length was calculated from 5 different FEG-SEM top-view and cross-section images and the standard deviation of the measurements was calculated from a minimum of ten measures of each parameter.

2.3. Photoelectrochemical characterisation

Electrochemical characterisation and PC and PEC activity were conducted in a three-electrode electrochemical cell shown in the supplementary information (Fig. 1S). For the determination of photocurrent densities by cyclic voltammetry (CV) and amperometric measurements, the anodised TiO_2-NTs electrodes were used as photoanode, a nickel mesh as the counter electrode and a Ag/AgCl (saturated in 3.0 M KCl) electrode acted as the reference electrode. Experiments were carried out using a total working volume of 0.4 L under stirring. The photoanode was placed perpendicular to four UVA lamps (Philips TL 6 W), with a maximum emission of 365 nm and an incident photon flow of 0.70 W·m^{-2}. Measurements were recorded at a scan sweep of 0.5 mV·s^{-1} between 0 and +1.4 V during 4 cycles with a potentiostat Eco-Chemie μAUTOLAB Type III. Amperometric measurements were recorded during the photoelectrocatalytic reactions at the potential bias (depending on the experiment between 0 and +1 V). The electrolyte consisted of a 0.1 mol·L^{-1} NaCl + 1 mol·L^{-1} CH_3OH aqueous solution, although in some experiments, the concentration of NaCl varied depending on the experiments. The recorded photocurrent values were transformed into photocurrent densities by considering the irradiated or photoactive surface of the electrodes (19.64 cm^2).

2.4. PC and PEC activity experiments

The PC and PEC runs were carried out always according to the following procedure. After the addition of a specific amount of NaCl in distilled water to prepare 0.4 L of electrolyte, 1.0 mol·L^{-1} of CH_3OH or 10^6 CFU·mL^{-1} of the microorganism (*E. coli*, *E. faecalis* or *C. albicans*) is added to the electrolyte. Then, in the PC experiments, the electrodes were placed in the cell without connection to the power supply, while for the PEC experiments, an external potential bias was applied between the working and the counter electrode. PEC reaction starts after switching on the light source and the external power supply. In the case of photochemical or photoelectrochemical experiments, a non-anodised titanium foil was used instead of the TiO_2-NTs electrodes. All the experiments were done with a magnetic stirrer at 300 rpm. Total illumination time was 90 min, adjusting the sampling time to the speed of the process.

Experiments of methanol oxidation in excess (1 mol·L^{-1}) were followed through the colorimetric determination of the formaldehyde at 412 nm following Nash's method (Nash, 1953). The kinetics of this reaction follows a well-known zero-order equation that can be adjusted to get the rate constant *k* (Marugán et al., 2010; Pablos et al., 2014).

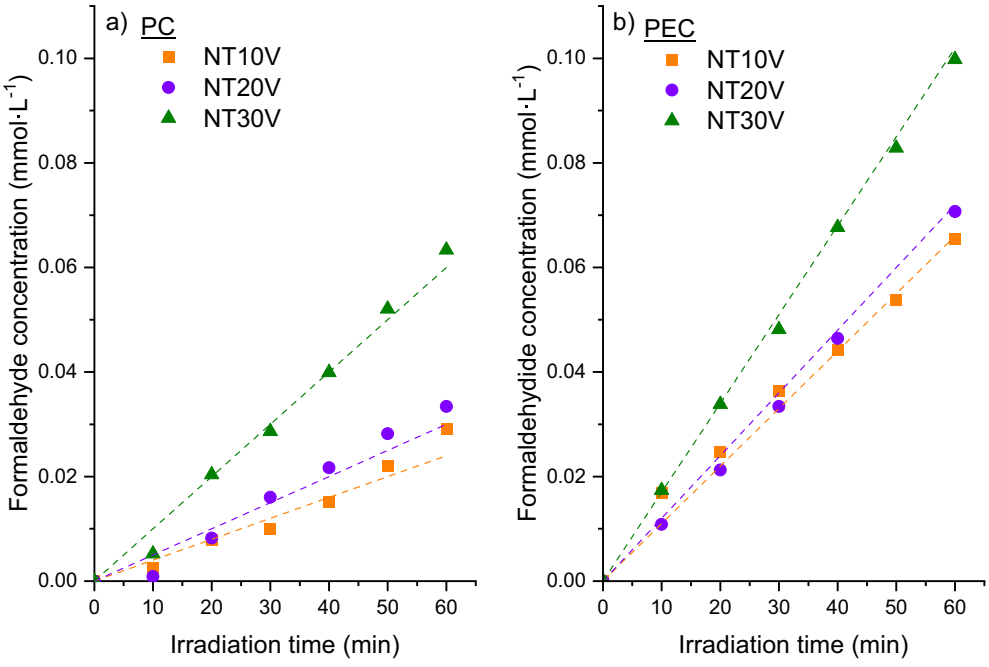

Fig. 1. PC and PEC formaldehyde production as a function of time in an electrolyte of 0.1 mol·L^{-1} NaCl + 1 mol·L^{-1} CH_3OH with the TiO_2-NT10V, TiO_2-NT20V and TiO_2-NT30V electrodes. Dashed lines correspond to the linear fitting of the experimental data.

The detection of active chlorine species was carried out by means of the orthotolidine-arsenite colourimetric method. This method allows for differentiating and evaluating the free residual chlorine, and the combined chlorine in the presence of interfering substances (nitrites, ferric or manganic compounds). Under well-determined time conditions and in an established order, the addition of orthotolidine and reducing agents produces a yellow colouration that is measurable by UV–visible liquid spectroscopy at the wavelength of 440 nm (APHA (American Public Health Association), 2012).

The analysis of the different samples collected for the formaldehyde and chlorine measurements was performed immediately in a UV–visible Spectrophotometer Biochrom LibraS22 spectrometer using a quartz sample holder of 1 cm optical path.

Measurements of pH and conductivity were made at the beginning and the end of all the reactions. The pH measurement has been carried out with a CRISON equipment model Compact Titrator GLP 22 while the conductivity measurements have been made with a CRISON conductimetre, model EC-Meter-Basic 30+.

For microbial inactivation experiments, three strains provided by the Spanish Type Culture Collection were used: *Escherichia coli* K12 (CECT 4624, corresponding to ATCC 23631) *Enterococcus faecalis* (CECT 5143, corresponding to ATCC 11700) and *Candida albicans* (CECT 1394, corresponding to ATCC 10231).

E. coli is frequently used as a model organism in microbiology studies and it is a common faecal contamination indicator to evaluate the microbiological quality of water. Fresh liquid cultures with a stationary concentration of around 10^9 CFU·mL^{-1} were prepared by inoculation in a Luria–Bertani nutrient medium (Miller's LB Broth, Scharlab) and incubation at 37 °C for 24 h under constant stirring on a rotary shaker, being diluted to the initial concentration of bacteria required for the experiments. The analysis of the samples along the reaction was carried out following the concentration of viable bacteria through a standard serial dilution procedure and agar plating, using eight independent measurements of each sample to obtain statistically significant data. To representate the figures, it was used the average of the viable bacteria concentration versus the reaction time and the standard deviation is represented by the error bars of each point. Saline water (NaCl 0.1 mol·L^{-1}) was used to do the dilutions and during all the experiments to avoid osmotic bacteria stress.

E. faecalis was cultured in 50 mL of Tryptic Soy Broth (TSB) incubated at 37 °C for 18 h. This culture (1 mL) was used to inoculate 10 L of water. Concentrations of *E. faecalis* in the diluted samples were enumerated by spreading 0.1 mL of Tryptic Soy Agar (TSA) on Agar plates, which were incubated at 37 °C for 24 h in an aerobic atmosphere.

The yeast *C. albicans* was incubated in TSB between 3 and 5 days at 25–30 °C for its growth and plated on Petri dishes with TSA for 48 h at 30 °C after the reaction.

3. Results and discussion

3.1. Characterisation and selection of the most active photoanode

The three prepared electrodes TiO_2-NT10V, TiO_2-NT20V and TiO_2-NT30V were tested in the oxidation of methanol in excess at +1 V in a 0.1 mol·L^{-1} NaCl electrolyte. Fig. 1. shows the formaldehyde concentration as a function of time in the PC and PEC reactions with the three TiO_2-NTs photoanodes (TiO_2-NT10V, TiO_2-NT20V and TiO_2-NT30V). PC and PEC oxidation of methanol experiments produces formaldehyde. The formaldehyde concentration displays a linear tendency that is adjusted to a zero-order kinetic equation to obtain the rate constant *k* from the slope following a well-established procedure (Pablos et al., 2014). In general, rate constants *k* obtained in PEC experiments ($16.6 \pm 0.2 \cdot 10^{-7}$, $12.9 \pm 1.1 \cdot 10^{-7}$, $10.4 \pm 0.5 \cdot 10^{-7}$ mol·L^{-1}·min^{-1}) are superior (almost double) than those of PC ($10.8 \pm 0.4 \cdot 10^{-7}$, $6.0 \pm 0.3 \cdot 10^{-7}$, $4.8 \pm 0.4 \cdot 10^{-7}$ mol·L^{-1}·min^{-1}) for the TiO_2-NT30V, TiO_2-NT20V and TiO_2-NT10V photoanodes, respectively. This fact confirms that the application of an external potential bias separates the anodic and cathodic reactions reducing the recombination of the electron-hole charges and increasing the rate constant (Pablos et al., 2014; Adán et al., 2016). Nevertheless, the TiO_2-NT30V sample achieves higher kinetic constants in both PC and PEC reactions than the TiO_2-NT20V and TiO_2-NT10V photoanodes. These results are consistent with the data obtained from the X-ray diffraction and Raman spectroscopy and scanning electron microscopy characterisation of these electrodes.

For the determination of the appropriate calcination temperature to get the anatase crystalline phase of TiO_2, the electrode TiO_2-NT20V was calcined using a temperature ramp from 30 to 600 °C. Fig. 2 shows the X-ray diffractograms as a function of temperature. As it is observed, from 30 °C to 300 °C only the diffraction peaks corresponding to metallic titanium appear at positions $2\theta \approx 35.1°$, 38.5°, 40.5° and 53.5°, according to the pattern (α-Ti 01–089-2762). It is from 350 °C onwards that the appearance of the most intense peaks of the anatase crystalline phase of TiO_2 assigned to the positions $2\theta \approx 25.5°$, 37.1°, 48.3° and 55.3°, begins to be observed (Anatase pattern 01-083-2243). When the calcination temperature reaches 550 °C, the formation of the rutile crystalline phase of TiO_2 is also observed by the appearance of the most intense peak at $2\theta \approx 27.4°$ (Rutile pattern 01-077-0444). Taking this into account, the electrodes used in this work were calcined at 450 °C.

Fig. 3.a shows Raman analysis which indicates the existence of the anatase crystalline phase of TiO_2 as can be corroborated by the six active modes located approximately at frequencies of 144 cm^{-1} (E_g), 197 cm^{-1} (E_g), 339 cm^{-1} (B_{1g}), 513 cm^{-1} (A_{1g}), 519 cm^{-1} (B_{1g}) and 639 cm^{-1} (E_g) (Balaji et al., 2006; Kalantar-zadeh et al., 2009;). On the other hand, higher anodisation potential results in an increase in the intensity of the Raman bands related to an increase in the thickness of the layer and/or length of the TiO_2 also confirmed by the FEG-SEM images measurements. In the same line, Fig. 3.b confirms the relationship between the length of nanotubes and the activity of the electrodes in the degradation of methanol. Methanol degradation rates in both curves grow linearly at a rate of $2.5 \cdot 10^{-7}$ mol·L^{-1}·min^{-1} for every μm of nanotube length. Fig. 4 shows the cross section and surface images from the three anodised electrodes. In addition, the external and internal diameters, the thicknesses of the wall and the lengths of the nanotubes for each electrode are collected in Table 1. Morphological analysis confirms the observations performed by Raman spectroscopy. Interestingly, the NTs length grows linearly from

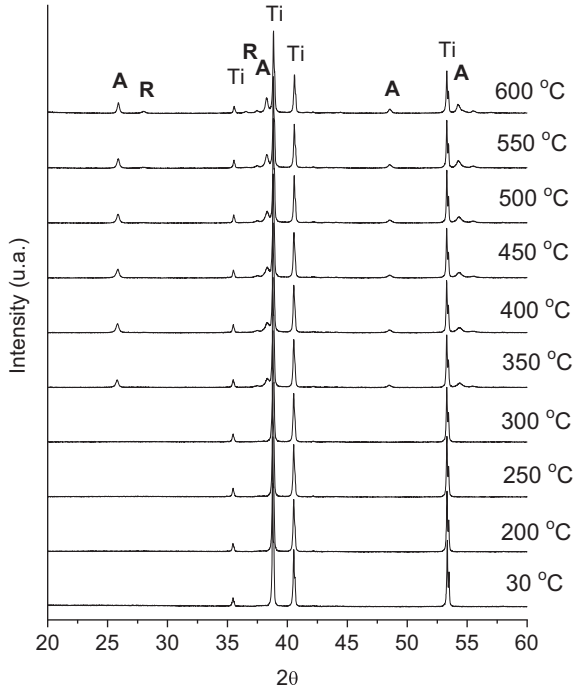

Fig. 2. X-Ray diffractograms of the TiO_2-NT20V electrode calcined at increasing temperatures.

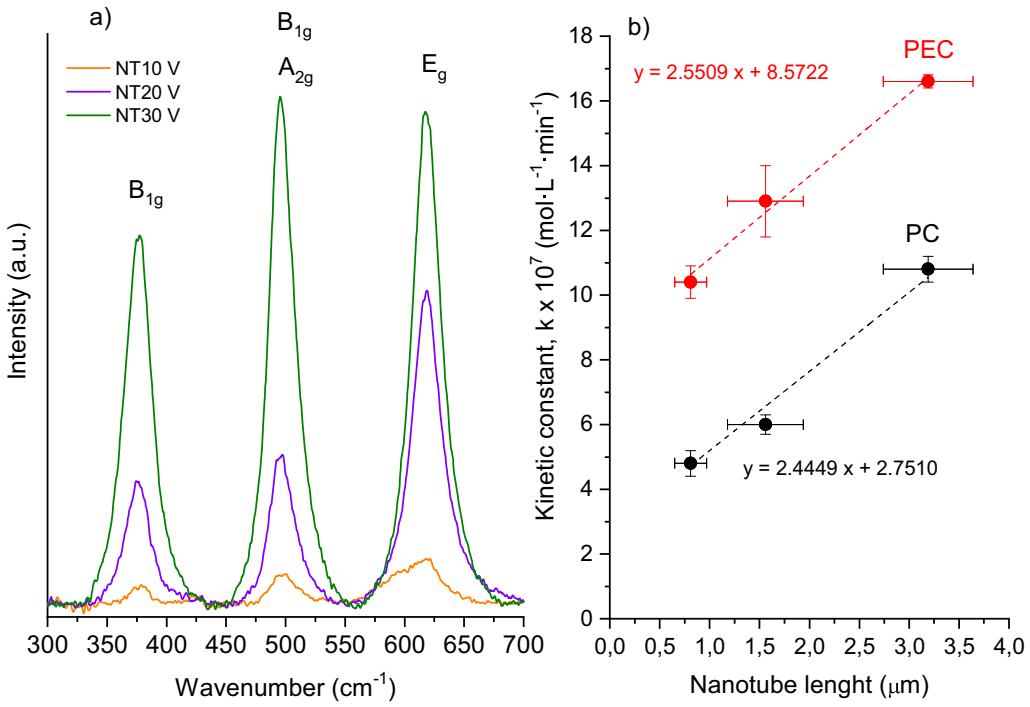

Fig. 3. a) Raman spectra of the TiO_2-NT10V, TiO_2-NT20V and TiO_2-NT30V electrodes and b) relation between kinetic constants for methanol oxidation versus nanotube length. Error bars for the kinetic constant calculated from the fitting error. The average nanotube length and standard deviation error bars were calculated from at least ten measurements.

0.81 ± 0.16, 1.56 ± 0.38 and 3.19 ± 0.45 μm as the applied potential increases as observed in a previous work (Adán et al., 2016). As well, the external diameter increases from 40 nm to 90 nm and the internal from 25 nm to 65 m, when anodisation potential grows from 10 to 30 V, while the wall thickness of the nanotubes remains practically constant between 20 and 30 V with a value of around 10 nm.

Although all the morphological parameters of the nanotubes increase as anodisation potential increases during synthesis, the length of the NTs is the most influential parameter in the kinetics of methanol oxidation (Adán et al., 2016). This fact is also confirmed in Fig. 5.a and b. where an increase in the length of the NTs increases the values of photocurrent intensity since the greater amount of photocatalyst gives rise to an increase in the capture

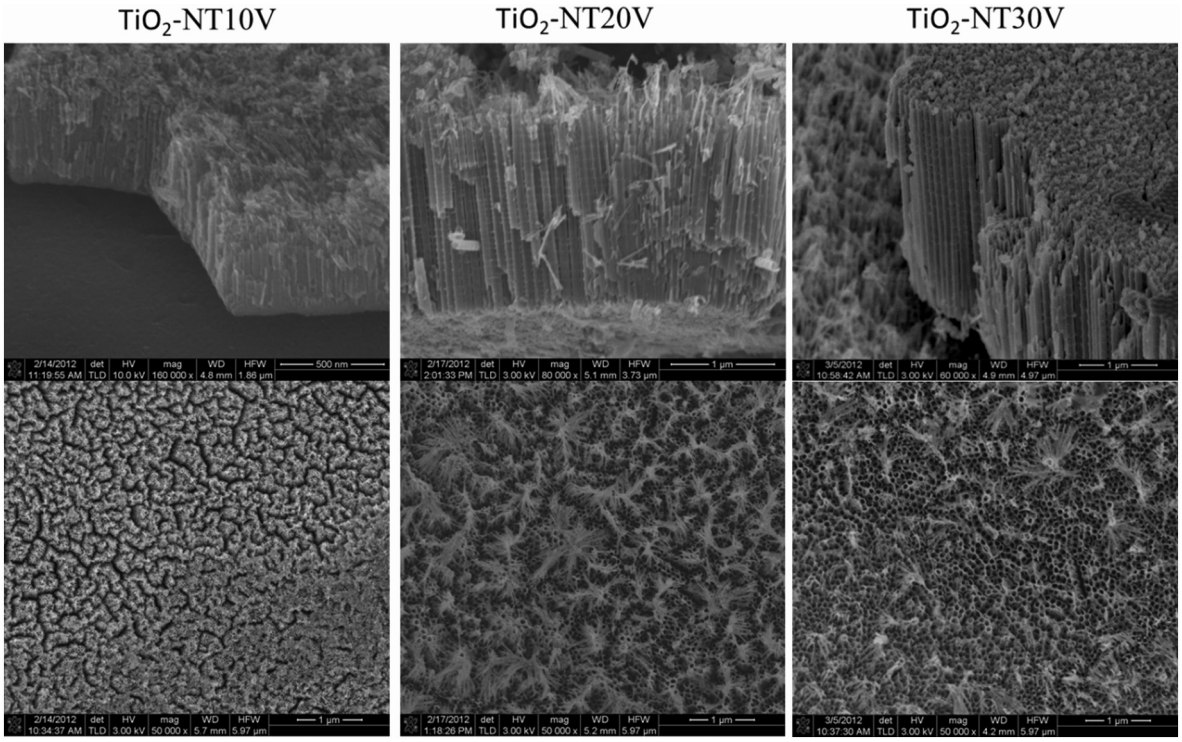

Fig. 4. FEG-SEM micrographs from the cross-section and surface of the TiO_2-NT10V, TiO_2-NT20V and TiO_2-NT30V electrodes.

Table 1
Morphological parameters of the TiO_2-NTs calculated from the FEG-SEM images of the electrodes TiO_2-NT10V, TiO_2-NT20V and TiO_2-NT30V.

Name	Inner diameter (nm)	Outer diameter (nm)	Wall thickness (nm)	Length (μm)
TiO_2-NT10V	26.9 ± 1.6	40.4 ± 3.4	5.5 ± 1.2	0.81 ± 0.16
TiO_2-NT20V	48.8 ± 6.4	69.1 ± 6.9	10.1 ± 1.5	1.56 ± 0.38
TiO_2-NT30V	71.3 ± 4.9	92.8 ± 4.8	10.8 ± 2.2	3.19 ± 0.45

of photons responsible for the generation of reactive species. The maximum photocurrent intensity is reached for an applied potential bias value higher than +0.4 V. The electrons will migrate to the cathode and carry out reduction reactions, while the holes will remain in the anode and oxidise the organic matter, thus achieving lower recombination of the charges and greater efficiency that is related to the observed intensity increase of photocurrent (Pablos et al., 2014; Adán et al., 2016). Therefore, it would be expected that a higher photocurrent density could offer a greater photocatalytic activity (Gong et al., 2010). On the other hand, the recorded photocurrent intensity was even greater in an electrolyte with 1 mol·L^{-1} methanol since methanol acts as a gauge of holes in the surface of the electrode, avoiding the recombination of the electron-hole pair and favouring the transfer of charge.

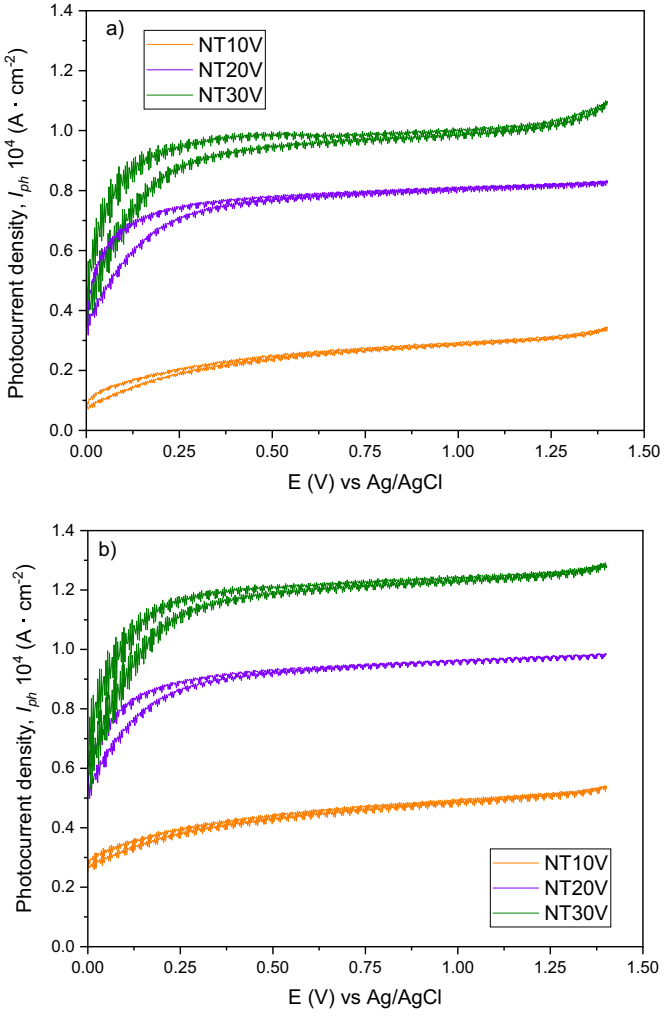

Fig. 5. Photocurrent densities, I_{ph}, recorded at a sweep rate of 0.5 mV s^{-1} for the TiO_2-NT10V, TiO_2-NT20V and TiO_2-NT30V electrodes in an electrolyte of a) 0.1 mol·L^{-1} NaCl and b) 0.1 mol·L^{-1} NaCl +1 mol·L^{-1} of CH_3OH. Incident photon flow of 0.70 W·m^{-2}.

3.2. PC and PEC activity with *E. coli*

Fig. 6 shows the results for *E. coli* inactivation together with the photolysis reaction (Ti electrode without NTs) and the photoelectrolysis reaction (Ti electrode without NTs and with the application of an external potential bias of +1 V). The photolysis and/or photoelectrolysis experiments are practically nil. In the same line, PC reaction gives rise to no more than one order of magnitude of reduction of viable bacteria. However, *E. coli* inactivation increases as a potential bias of +1 V are applied to the electrodes. In addition, all the electrodes show total inactivation of the *E. coli* after 7, 15 and 150 min of irradiation with the TiO_2-NT30V, TiO_2-NT20V and TiO_2-NT10V electrodes respectively, reaching the detection limit of bacteria (dashed line). For quantitative analysis, each *E. coli* inactivation profile have been fitted to a first-order kinetic model to compare the kinetic constants of the different reaction conditions studied.

PC experiments display similar activity with kinetic constants very low with similar values to the photolysis and photoelectrolysis experiments. In the case of PEC experiments, kinetic constants are all much higher, being 0.124, 1.103 and 2.465 ·min^{-1} for the TiO_2-NT10V, TiO_2-NT20V and TiO_2-NT30V, respectively.

However, the results achieved from PC and PEC during the inactivation of *E. coli* are not compensated. In methanol oxidation, the application of a positive potential bias reduces the recombination of the electron-hole pairs photogenerated and increases the reaction rates from the PC, almost doubling its *k* value while in the case of *E. coli* inactivation, the differences between PC and PEC *k* values are even much bigger. Fig. 7 shows the relation between the kinetic constant in the inactivation of *E. coli* and the length of nanotubes for PC and PEC experiments. Contrary to what it is observed in Fig. 3.b, where the kinetic constants of methanol degradation grow in parallel between the PC and PEC experiments, the value of kinetic constants for the inactivation of bacteria significantly differ as the length of the nanotubes increases, reaching in case of the TiO_2-NT30V photoanode, values about 630 times higher than in the photocatalytic process. Therefore, it is clear that in the inactivation of bacteria, microbiological factors not present in the oxidation of methanol, are being decisive. In these experiments, the detection of active chlorine can justify the higher inactivation rates observed during PEC reactions. Fig. 8 shows the total, free and combined chlorine concentrations measured during the tests. Fig. 8.a shows the chlorine values detected after reaching total inactivation of *E. coli* during PEC experiments at times of 7, 15 and 150 min for the TiO_2-NT30V, TiO_2-NT20V and TiO_2-NT10V respectively. Total chlorine concentration reaches

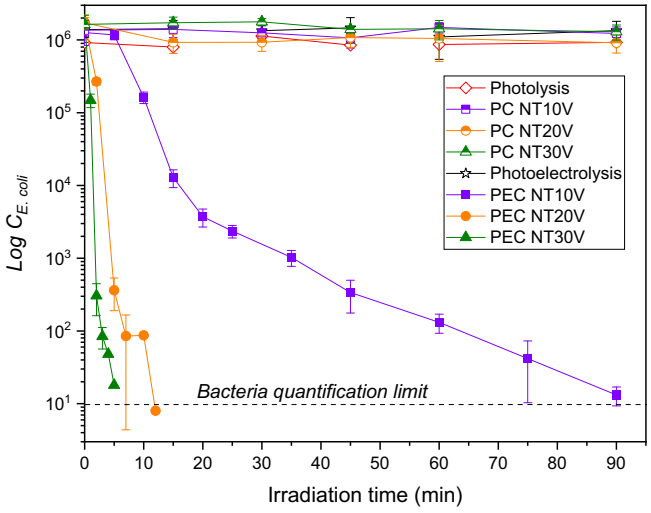

Fig. 6. PC and PEC inactivation of *E. coli* with the TiO_2-NT10V, TiO_2-NT20V and TiO_2-NT30V electrodes in a 0.1 mol·L^{-1} NaCl electrolyte, initial *E. coli* concentration of 10^6 CFU·mL^{-1} and potential bias of +1.0 V. Incident photon flow of 0.70 W m^{-2}. Error bars were calculated from eight independent bacterial counts.

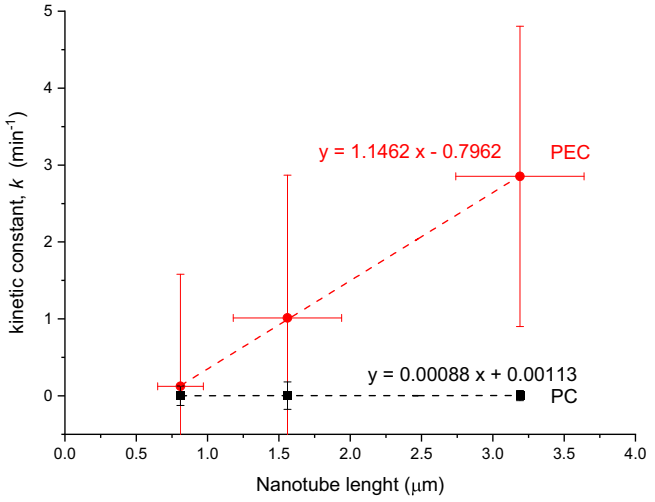

Fig. 7. Relation between kinetic constants for *E. coli* inactivation vs nanotube length. Error bars for the kinetic constant calculated from the fitting error. The average nanotube length and standard deviation error bars were calculated from at least ten measurements.

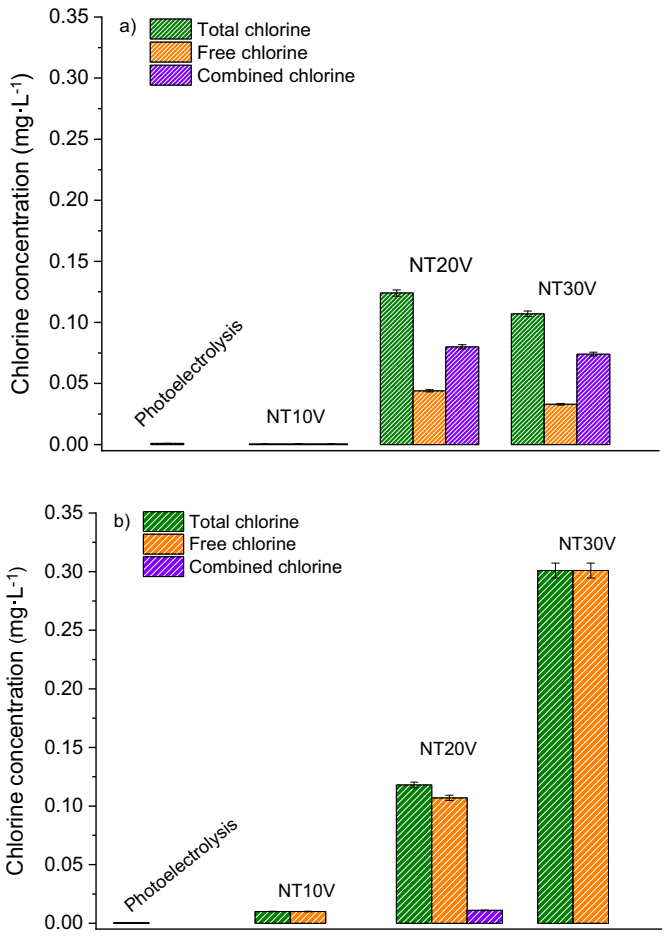

Fig. 8. Concentration of chlorine species a) at the end of the PEC reactions with *E. coli* (at times of 7, 15 and 150 min for the TiO_2-NT30V, TiO_2-NT20V and TiO_2-NT10V electrodes, respectively) and b) at 30 min irradiation without the addition of *E. coli*. Error bars correspond to the relative experimental error of each measurement (2 %).

0.12 mg·L^{-1}, similar in both TiO_2-NT20V and TiO_2-NT30V electrodes. These results have a significant effect on the inactivation of *E. coli* since a greater concentration of chlorine species was detected in the electrodes that reached better results in bacterial inactivation. In the case of the TiO_2-NT10V electrode, practically no chlorine species were detected at the end of the experiment in line with the PEC results. It is interesting to note that under these experimental conditions, chlorine production was undetectable during the photolysis, photoelectrolysis and PC reactions as well as in dark conditions, demonstrating that for the in-situ generation of active chlorine under our experimental conditions is necessary the combination of TiO_2, an external potential bias and UVA illumination.

For better understanding, chlorine was measured under the same reaction conditions without adding bacteria. Fig. 8.b shows chlorine species concentrations detected after 30 min in the PEC experiments without *E. coli* addition. In this case, the concentration of chlorine species in the electrolyte increases in TiO_2-NT10V, TiO_2-NT20V and TiO_2-NT30V electrodes progressively with irradiation time and reaches a maximum of 0.3 mg·L^{-1} with the TiO_2-NT30V electrode as the chlorine is not consumed in the reaction during the contact with the bacterium. It should be noted that the greater production of chlorine is directly related to the greater amount of TiO_2 i.e., with the higher length and diameter of the nanotubes, as shown in Table 1. When comparing the results from Fig. 8.a and b, the amount of total, free and combined chlorine follow a different route. In Fig. 8.a the concentration of free chlorine decreases to be transformed into combined chlorine when *E. coli* structures start degrading while in Fig. 8.b, all the chlorine is in the form of free chlorine and is longer accumulated. These values follow the results of Hoff et al. (Hoff and Akin, 1986) who studied the effect of free chlorine on different types of microorganisms under different conditions. This work demonstrated that free chlorine concentrations >0.05 mg·L^{-1} at 20–29 °C and pH 7 were enough to reach a 99 % of inactivation of *E. coli* in approx. 2 min of contact, while with a higher pH of 8.5 higher concentrations of free chlorine of around 0.3 mg·L^{-1} were necessary to inactivate *E. coli* in less than two minutes.

On the other hand, although the specific measurements of chlorine carried out on the NT10V electrode, showed that practically no chlorine species were detected in any case (Fig. 8.a and b), when chlorine species concentrations evolution is monitored, (Fig. 9) it is observed a maximum of approx. 0.45 mg·L^{-1} of combined chlorine at 15 min that disappears with the irradiation time. Some authors pointed out that active chlorine production is faster in the first 15 min of the process and then reaches a maximum value after a longer period, suggesting that maximum saturation has been attained in addition to the expected limitation imposed by the geometric area of the electrode (Zanoni et al., 2004; Cheng et al., 2007; Fraga et al., 2009). After these 10–20 min, combined chlorine decreases and does not exceed 0.1 mg L^{-1}. In parallel, it is observed that the maximum concentration of chlorine detected concurs with a sharp drop in the *E. coli* curve and from that point, chlorine is consumed appreciating a decrease in the smoother curve. As well, control over pH can be a critical factor in determining the degree of disinfection achieved by a certain level of free chlorine. Taking into account the pH of these experiments (pH ~ 8.5) it can be stated that a low or moderate generation of chlorine is expected and also, the predominant species of the chemical equilibrium will be the hypochlorite ion (OCl^-), which is about 80–100 times smaller than the disinfecting ability of hypochlorous acid, predominant specie at acid pH (García-Espinoza et al., 2021).

It is interesting to note that active chloride species were also measured in methanol oxidation reactions, although the presence was undetected, neither in the PC nor in PEC reactions. This can be explained as the methanol, which is in excess in these reactions, can act as a hole trapping agent or scavenger. As it was discussed, h^+ starts the direct and indirect oxidation route therefore, it is the most critical factor. Thus, h^+ scavenging might be a potential way to block chlorine generation (Chi et al., 2020).

3.3. Application of an external potential bias

According to the screening results of the electrodes, TiO_2-NT30V was selected to evaluate the photoelectrocatalytic experiments in the

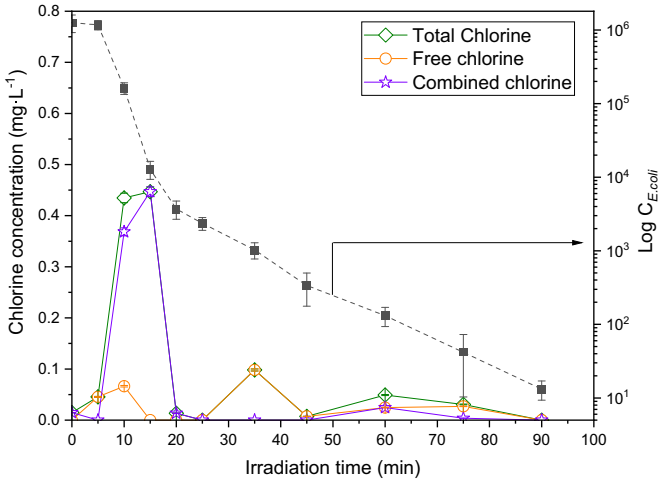

Fig. 9. Evolution of the concentration of chlorine species during the photoelectrocatalytic inactivation of *E. coli* measured with the TiO_2-NT10V electrode. Conditions: 0.1 mol·L^{-1} NaCl electrolyte, initial *E. coli* concentration of 10^6 CFU·mL^{-1}, potential bias of +1.0 V an incident photon flow of 0.70 W·m^{-2}. Error bars were calculated from eight independent bacterial counts.

degradation of methanol and bacteria at different potential values. Fig. 10.a shows the influence of increasing the applied potential bias from −0.2 to +1 V on the oxidation rate of methanol whereas Fig. 10.b shows the photocurrent intensity registered at 60 min versus potential bias. The dashed line represents the value of the kinetic constant that was obtained in the PC reaction during methanol oxidation.

Potentials between +0.4 and +1 V present very similar kinetic constants since, at values somewhat higher than +0.4 V, the maximum photocurrent intensity was obtained, in agreement with other authors (Zanoni et al., 2004; Adán et al., 2016). The kinetic constants reached in the degradation of methanol are always higher than the kinetic constant of the PC reaction (dashed line) except in the experiment where the application of an external potential bias of −0.2 V where the kinetic constant is slightly lower. This is because positive potential bias separates anodic and cathodic reactions reducing the recombination of electron-hole pairs, which is avoided in the experiment −0.2 V (Zanoni et al., 2004). The kinetic constant reached at 0 V is even higher than that obtained in the PC reaction, since the system works in a closed circuit and allows the transfer of electrons to the cathode, thus decreasing the activation energy of the reduction reaction (controlling process) and increasing the overall speed of photooxidation (Pablos et al., 2014; Adán et al., 2016).

Fig. 11.a shows PEC kinetic constant for the inactivation of *E. coli* vs external potential bias applied to the TiO_2-NT30V electrode. In general, between 2 and 6 min, inactivation of *E. coli* reached 99.99 % applying a positive potential bias between 0 to +1 V in all the experiments. Photoelectrolysis and the experiment with −0.2 V potential bias display very low kinetic constants. However, as the external potential bias increases, kinetic constants from *E. coli* inactivation also increases until reaching a plateau above +0.4 V. On the other hand, at 0 V is reached a kinetic constant of 0.967 min^{-1} which demonstrates that the TiO_2-NT30V has some photoelectrochemical activity in a closed circuit (six orders of magnitude of *E. coli* inactivation are reached at 15 min of irradiation), as it happened with the degradation of methanol in Fig. 10.a. allowing the transfer of electrons from the anode to the cathode (Adán et al., 2016).

Fig. 11.b represents the concentration of chlorine species accumulated at 30 min without *E. coli*. As the external potential bias increases the chlorine concentration also increases until it reaches a maximum of around 0.32 mg·L^{-1} in agreement with other reports (Zanoni et al., 2004; Fraga et al., 2009). However, although some small differences are observed between the chlorine concentrations from +0.4 V to +1 V, *E. coli* inactivation is practically reached at the same time in line with the maximum photocurrent intensity achieved in these electrodes (see Fig. 5). On the other hand, it is appreciated that with the photoelectrolysis and the application of a negative potential (−0.2 V) no chlorine is produced, confirming that the combination of small concentrations of chlorine such as 0.1 and 0.2 mg·L^{-1} and the PEC process is capable of inactivating up to 10^6 CFU·ml^{-1} of bacteria in <15 min.

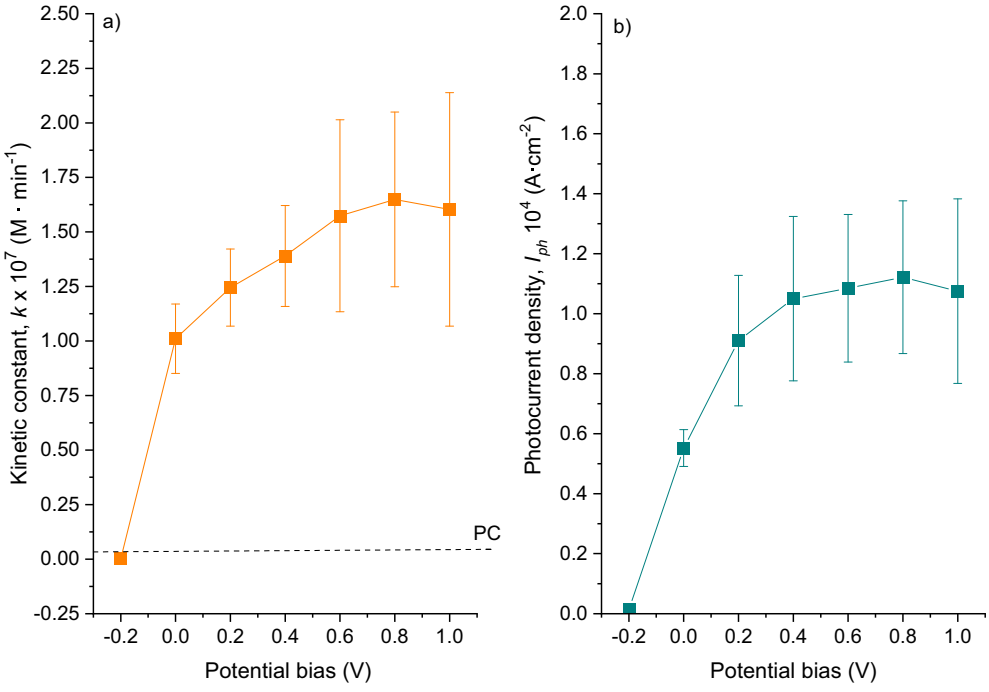

Fig. 10. a) Influence of the applied potential bias (from −0.2 to +1.0 V) on the values of the zero-order kinetic constant of formaldehyde production measured in the NT30V electrode. and b) photocurrent density measured at 1 V from voltamperometric. Incident photon flow of 0.70 W·m^{-2}.

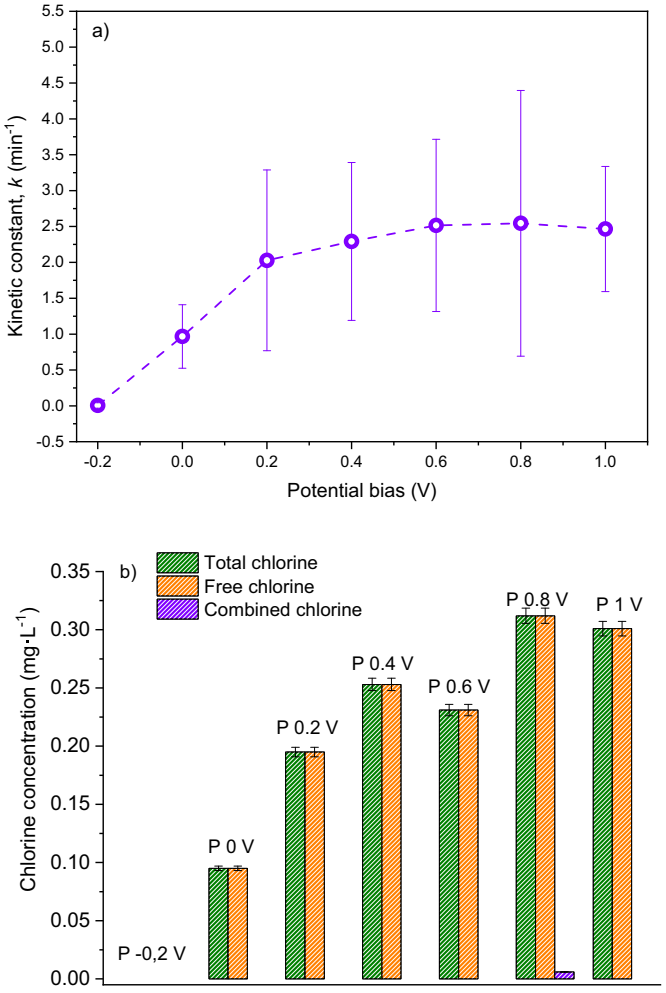

Fig. 11. a) Kinetic constants for *E. coli* inactivation at different potentials bias measured with the NT30V electrode. Conditions: 0.1 mol·L^{-1} NaCl electrolyte, initial *E. coli* concentration of 10^6 CFU·mL^{-1}. Error bars are the standard error from the kinetic constant. b) Chlorine species quantification in PEC at 30 min without *E. coli*. Error bars correspond to the relative experimental error of each measurement (2 %).

3.4. Effect of chloride ions concentration

The parameters and the kinetic constants calculated from the oxidation of methanol with a NaCl electrolyte containing different concentrations of the salt (from 0 to 0.15 mol·L^{-1}) as a function of time are collected in Table 2. Notably, the kinetic constant remains practically unaltered, as well as photocurrent density at +1 V. In contrast with other studies (Zanoni et al., 2004), an increase in photocurrent was not observed as the amount of Cl^- increases, probably because at pH 8.5, these differences are not as significant as at pH 4. As expected, as Cl^- concentration increases also increase the electrolyte conductivity at a rate of 0.0865 mS·cm^{-1}. Distilled water displays a pH value of around 6, while with different Cl^- concentrations, the pH is around 8.5–8.8. Other authors (Zhang et al., 2005) have studied the effect of Cl^- concentration on the degradation of reactive Brilliant Orange K-R (RBOKR). They observed that as the conductivity of the solution increase (from 0.5 to 47.2 mS·cm^{-1}), the photoelectrocatalytic process can be more efficient even than direct electrooxidation and photocatalytic oxidation processes, demonstrating that the efficiency of the photoelectrocatalytic process was not only greater than that of the photocatalytic or electrochemical process but also greater than the sum of the two processes. These authors recognise that the reason for this enhancement can be due to the reached equilibrium achieved in the adsorption of Cl^- ions at high Cl^- ions concentration or due to the generation of active chlorine.

On the other hand, Fig. 12.a shows the values of the kinetic constants calculated from bacterial inactivation curves with increasing amounts of chloride ions in the electrolyte. It is noted that the inactivation of *E. coli* increases rapidly from 0 to 0.12 mmol·L^{-1} concentration of Cl^- although the increase in the kinetic constant with Cl^- concentrations above 4 mmol·L^{-1} is not that pronounced. Kinetic constants from Fig. 12.a demonstrate that *E. coli* inactivation activity slightly increases as Cl^- concentration increases, tending to reach a plateau. Anyway, although the kinetic constant slightly increases, the changes in Cl^- concentration from 15 to 150 mmol·L^{-1} have no noticeable effect on the inactivation efficiency as with the addition of 15 mmol·L^{-1} or higher amounts of Cl^-, 99.99 % of inactivation is reached at times lower than 4 min in all the tests.

This fact is confirmed with Fig. 12.b, where the concentration of active chlorine at 30 min of irradiation time without any bacterium versus kinetic constants is represented. With low concentrations of Cl^- (<0.12 mmol·L^{-1}), there is almost no detection of free chlorine, while

Table 2
Kinetic constants, conductivity at 20 °C, photocurrent intensity and initial and final pH recorded during the PEC TiO_2-NT30V experiments with 1 mol·L^{-1} methanol with different Cl^- concentrations.

Cl^- concentration (mmol·L^{-1})	k (mol·L^{-1}·min^{-1}) ×10^7	Photocurrent density at +1.0 V (mA)	Conductivity (mS·cm^{-1})	pH
0.0	10.42 ± 0.44	–	0.017	5.8 ± 0.5
0.12	10.86 ± 0.36	0.0024	0.15	8.8 ± 0.2
4	12.43 ± 0.41	0.0022	0.34	8.5 ± 0.3
15	11.87 ± 0.39	0.0022	1.42	8.8 ± 0.2
60	12.63 ± 0.65	0.0020	5.42	8.7 ± 0.2
105	11.78 ± 0.30	0.0022	8.85	8.5 ± 0.2
150	11.87 ± 0.21	0.0022	13.18	8.4 ± 0.3

Conductivity correlation vs Cl- concentration: Y = 0.0865X + 0.0696; R^2 0.999.

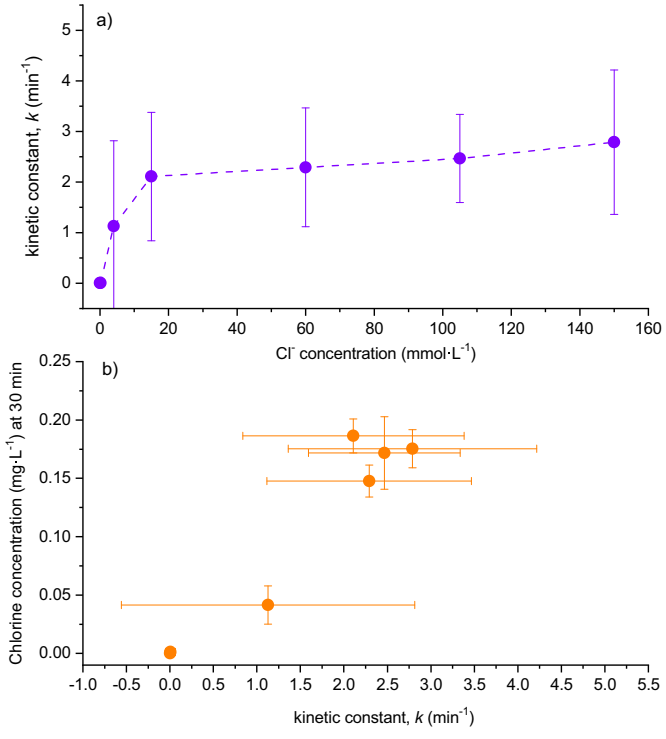

Fig. 12. a) Kinetic constants from the PEC inactivation of *E. coli* at different NaCl concentrations measured in the NT30V electrode. Conditions: initial *E. coli* concentration of 10^6 CFU·mL^{-1} and external potential bias of +1.0 V. Error bars are the standard error from the kinetic constant. b) Chlorine concentration measured at 30 min of irradiation time without the addition of *E. coli*. Chlorine error bars is the relative error from two repeated experiments.

with concentrations above 4 mmol·L^{-1} or higher, there is a slight increase in chlorine concentration of around 0.2 mg·L^{-1}. Chlorine concentrations are similar, but the constants continue increasing with the increase in Cl^-, which points out that other factors influence bacteria inactivation, such as the electrolyte conductivity, surface interaction with charge cations or the bacterial membrane behaviour with the osmolarity changes. Similar results have been published by other authors (Zanoni et al., 2004; Selcuk and Anderson, 2005; Cheng et al., 2007) in an acid pH medium. Cheng et al. (Cheng et al., 2007) studied three Cl^- concentrations on the removal of NO_2^- at pH 4.7 and +1.0 V. They observed that the rate of degradation of NO_2^- increases rapidly with increasing concentration of Cl^- from 100 to 500 mmol·L^{-1}. For instance, in the absence of NaCl, only 70 % of NO_2^-, was oxidised within 20 min, while adding 10 mmol·L^{-1} NaCl, complete degradation of NO_2^-, was achieved within 15 min and at a higher NaCl concentration of 500 mmol·L^{-1}, only 4 min is needed for completing degradation. In the same line, Xiao et al. (Xiao et al., 2019) followed the amount of free chlorine in the photoelectrocatalytic breakdown of Cu-cyanide complexes at pH 8.0 and applied a potential of +1.5 V with a WO_3 nanoplate film photoanode. They also observed that the concentration of free chlorine increases as the concentration of Cl^- increases from 0 to 30 mmol·L^{-1} reaching free chlorine concentrations higher than those reported in this work.

3.5. Type of electrolyte

Fig. 13.a represents *E. coli* inactivation constants at +1 V using an initial concentration of 10^6 CFU·mL^{-1} *E. coli* + 0.1 mol·L^{-1} NaCl or 0.1 mol·L^{-1} $CaCl_2$ or 0.1 mol·L^{-1} $NaSO_4$ as electrolyte.

Total inactivation of *E. coli* was reached at times <10 and 20 min with NaCl and $CaCl_2$ electrolytes, while only one order of magnitude was achieved in the $NaSO_4$ electrolyte after 30 min. Although a higher concentration of Cl^- is expected in the $CaCl_2$ electrolyte (210 mmol·L^{-1} of Cl^- vs 105 mmol·L^{-1} of Cl^- with the NaCl electrolyte), the greatest *E. coli* inactivation is observed using NaCl solution. Free chlorine has been detected in electrolytes with NaCl (0.35 mg·L^{-1}) and $CaCl_2$ (0.14 mg·L^{-1}) at 15 min reactions which explains the results obtained with these electrolytes. These experiments have corroborated that the formation of free chlorine can occur in any type of chloride electrolyte. Other authors have performed similar studies with common electrolytes, such as NaCl, Na_2SO_4, Na_2HPO_4 and $NaNO_3$, at different concentrations to determine their effects on microcystin-LR (MCLR) degradation with a RuO_2-TiO_2/Ti photoanode (Zhao et al., 2019). They observed that when NaCl was used as an electrolyte, the degradation effect of MCLR was better than with the non-chloride electrolytes. MCLR was completely degraded even with 2 mmol·L^{-1} NaCl after 30 min and was undetectable even after 5 min when NaCl increased to 20 mmol·L^{-1}. These results confirm that Cl^- can be adsorbed on the surface of the anode and be oxidised to highly active oxidative groups (•Cl, Cl_2 and HClO) by electron-hole pairs (Zhao et al., 2019).

Two possible explanations for the decrease in the inactivation constant of bacteria and chlorine generation for $CaCl_2$ electrolyte has been raised. On the one hand, the conductivity values can change from one electrolyte to another, expecting that a better conductivity can improve the photo electrocatalytic activity. However, it was expected that $CaCl_2$ would be the better electrolyte, which is confirmed by the conductivity achieved in $CaCl_2$ (15.05 mS · cm^{-1}), Na_2SO_4 (13.10 mS · cm^{-1}) and NaCl (8.85 mS · cm^{-1}) at 20 °C, since the conductivity of an electrolyte depends on the number of charges that are mobile within a solution, and $CaCl_2$ and Na_2SO_4 contain more charges than NaCl. Therefore, the conductivity does not seem to have a great influence on the formation of chlorine. On the other hand, other factor to be considered could be related to the interaction of the negative surface of TiO_2 (pH > pzc) with the positive cation Ca^{2+}. Some studies have demonstrated that TiO_2 shows affinity toward Ca compounds that can transform surface characteristics and modify the nanoparticles profile (Saygin and Baysal, 2022).

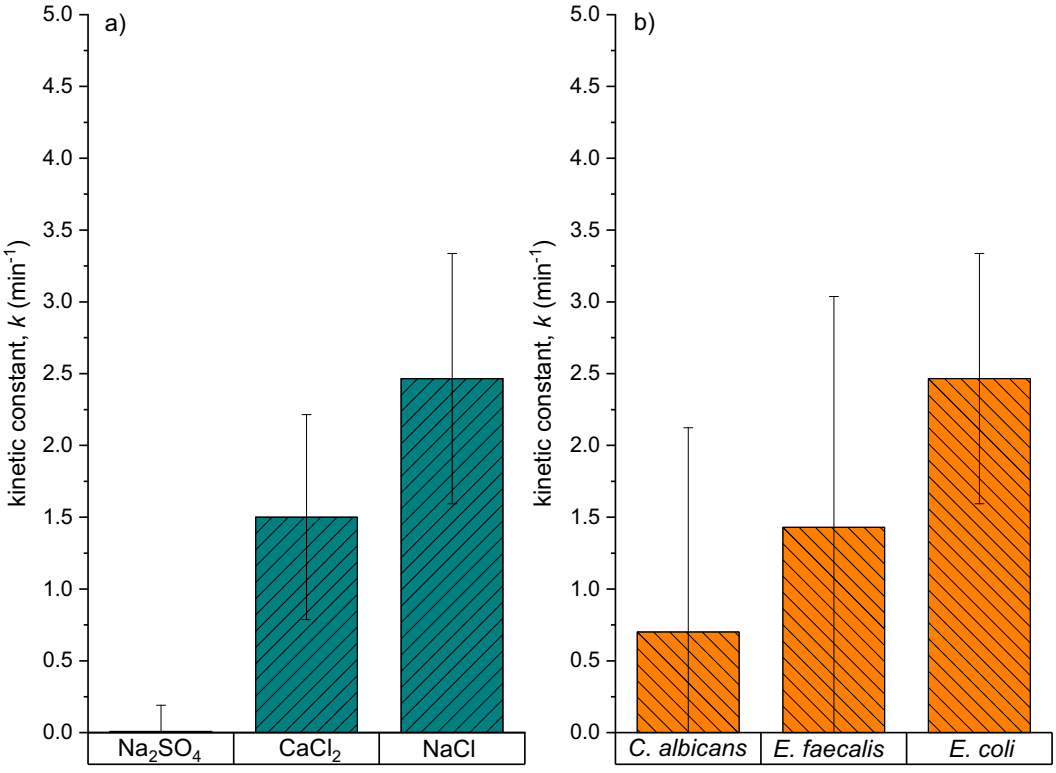

Fig. 13. a) PEC inactivation constants of *E. coli* with different electrolytes measured in the NT30V electrode. Conditions: 0.1 mol·L^{-1} electrolyte, initial *E. coli* concentration of 10^6 CFU·mL^{-1} and external potential bias of +1.0 V. b) inactivation of different microorganisms. Conditions: 0.1 mol·L^{-1} electrolyte, initial *E. coli* concentration of 10^6 CFU·mL^{-1} and external potential bias of +1.0 V. Error bars are the standard error from the kinetic constant.

3.6. Resistance of microorganisms

The TiO_2-NT30V electrode was evaluated in the inactivation of *E. coli, E. faecalis* and *C. albicans* at +1 V using an initial concentration of 10^6 CFU·mL^{-1} of microorganisms + 0.1 mol·L^{-1} NaCl.

Fig. 13.b shows the PEC kinetic constants with different microorganisms such as *E. coli, E. faecalis* and *C. albicans*, a fungus in the form of yeast responsible for pathogenic diseases such as vaginal candidiasis (vaginitis), oral cavity (Muguet), intestine or skin (O Young, 2016). The inactivation of *E. coli* occurs at shorter times than the inactivation of *E. faecalis* and that of the *C. albicans* fungus. These results are explained by considering the different morphological and structural characteristics of these microorganisms. It is well established that bacterial inactivation begins with the attack of the hydroxyl radicals formed by the photocatalyst on the membrane or cell wall (Pulgarin et al., 2012). Several attacks are needed to generate irreversible damage to the bacteria. Therefore, the more resistant this wall or outer layer is, the longer time will be required, and the higher number of attacks and radicals will be necessary for its complete inactivation. Bacteria *E. coli* and *E. faecalis* share the same genus but their cell wall is structurally different. *E. coli* is a Gram-negative bacterium while *E. faecalis* is Gram-positive. The cell wall of Gram-positive bacteria is composed of several layers of peptidoglycan (> 25 layers) that make up a thick and rigid structure, representing up to 90 % of the cell wall, which explains its higher resistance to inactivation. In contrast, the cell wall of Gram-negative bacteria, such as *E. coli*, is composed of a layer or few layers of peptidoglycan and an outer membrane. The fact that it contains a small amount of peptidoglycan in the cell wall increases its susceptibility to mechanical rupture, hence it is the bacteria with the least resistance to inactivation (van Grieken et al., 2010). On the other hand, the fungus has, in general, greater resistance than bacteria to biocides (Day et al., 2009; Vijayakumar and Sandle, 2019). Not all fungal species have cell walls, but if they do, they are composed of mannans, glucans and chitin (O Young, 2016). In *C. albicans* the outermost layers consist mostly of 1,6-mannan and 1,2-mannan while a third layer is of 1,6-glucan. As its structure gets deeper, 1,6-glucan changes to 1,3-glucan, which combines with chitin, ending with the innermost layers composed largely of chitin-protein (O Young, 2016). Chitin is a very resistant molecule that explains the greater resistance of fungi against disinfection processes.

On the other hand, it should be noted that apart from the attack of free radicals formed by the electrode during the reaction, the formation of chlorine also contributes to the inactivation of these microorganisms (García-Espinoza et al., 2021). Although the exact mechanism of the disinfecting action of chlorine is unknown, some studies propose that chlorine does not only exerts an oxidising action in the cell membrane and cell wall to destroy semi permeability but also reacts with internal RNA and destroys and/or inhibits the enzymatic systems on which microorganisms depend for the use of food, which causes them to die of starvation (Junli et al., 1997; Junli et al., 1997; Li et al., 2011; Li et al., 2013). In the case of PEC combined with active chlorine, there is a concomitant effect between the attack of chlorine species and the direct attack of the photohole to rapidly damage/decompose the cell body of the bacteria that is in contact with the photoanode surface (Li et al., 2011).

Chlorine values found for the disinfection of *E. coli, E. faecalis* and *C. albicans* in water chlorination are slightly higher than those obtained in the PEC process. Different studies have demonstrated that small amounts of active chlorine can inactivate *E. coli* and *E. faecalis*. For *E. coli*, 0.05 mg·L^{-1} of active chlorine at pH 7 was enough to reach 99 % of inactivation in 2 min of contact time while at pH 8.5 a concentration of chlorine of 0.3 mg·L^{-1} was necessary (Hoff and Akin, 1986). The photoelectrocatalytic chlorine generation of our work only needs 2–3 min to inactivate 99.99 % of *E. coli* at pH 8.5. In the case of *E. faecalis* higher concentration of chlorine was necessary. According to Ersoy et al. (Ersoy et al., 2019), 1.2 mg·L^{-1} of NaOCl and ClO_2 caused almost 70 % of inactivation in <1 min suggesting that cells may have problems with respiration and anabolism when treated with chlorine-based disinfectants. Our results show 99.99 % inactivation in 7 min. Finally, in the case of *C. albicans* it was necessary for an exposition to 0.2 mg·L^{-1} of chlorine for 3 h in tap water to reach the complete elimination of viable cells, while with higher concentrations of oxidant of 0.4 mg·L^{-1}, between 30 and 60 min of treatment were enough to obtain the same result (Sisti et al., 2012). In this work, PEC with NT30V achieved 99.99 % of inactivation of *C. albicans* in 15 min. Similar results were observed by Li et al. (Li et al., 2011), who worked with different pHs (from 5.6 to 9.3) on the percentage inactivation for PEC systems. These authors found that for the PEC–Cl treated samples under different pHs, the inactivation percentage moderately increased from 38.8 % to 52.5 % when pH increased from 5.6 to 7.4, but dramatically increased to 99.0 % when pH was further increased to 9.3, suggesting a significant contribution by AOSs at high pH. In summary, this work has demonstrated that in situ generation of chlorine with the PEC process can increase efficiency compared to traditional chlorination where chlorine is added and dissolved in the medium.

4. Conclusions

During the photoelectrocatalytic process used in water treatment conditions, active chlorine can be generated in a very low or even undetectable concentration, which in some cases, may cause overestimation of photoanode activity. Our findings indicate that chlorine can be easily generated in situ by direct oxidation of chloride ions on the PEC process with an electrode based on TiO_2/Ti nanotubes even in not favoured conditions.

The examination of different conditions including the applied current potential bias, concentrations of Cl^-, type electrolyte and type of microorganisms were evaluated with methanol and *E. coli*. This research has led to the following conclusions:

- PEC kinetic constants were always higher than the kinetic constant of the PC reactions. The increase in the length of the nanotubes has increased the PC and PEC activity in the degradation of methanol and bacterial inactivation, being most active the electrode with longer nanotubes (3.19 ± 0.45 μm).
- Similar kinetic constants were reached in the PEC experiments with methanol oxidation and *E. coli* inactivation by applying a potential bias of +0.4 V to +1 V, as the maximum intensity of photocurrent is reached in this range.
- Electrolytes with chloride salts are susceptible to the photoelectrocatalytic production of chlorine species, although results can vary depending on the type of salt employed. NaCl has resulted to be more effective than $CaCl_2$, probably due to the negative interaction between Ca^{2+} cations with the negatively charged surface of TiO_2.
- The formation of chlorine is higher as the length of the nanotubes increases and increases with higher Cl^- ion concentration. *E. coli* can be photoelectrocatalytically inactivated more effectively with higher solutions containing Cl^- ion from a value of 15 mmol·L^{-1} in contrast with the result observed for methanol oxidation.
- TiO_2-NT were a success in the inactivation of *E. coli. E. faecalis* and *C. albicans* by PEC, the results show a strong influence of the structure of the wall and microbial membrane on the efficiency of the inactivation process. Under equivalent conditions of electrolyte irradiation dose, the inactivation of *E. coli* is higher than *E. faecalis* and *C. albicans*.
- Small amounts of free chlorine can be generated under unfavourable conditions with the combination of TiO_2, the application of an external anodic bias and UVA illumination

This work has demonstrated that the TiO_2 nanotube electrodes through the photoelectrocatalytic process are adequate to achieve a total bacterial inactivation of microorganisms in a short period and obtain a good degradation of organic compounds, such as methanol.

CRediT authorship contribution statement

Cristina Adán: Conceptualization, Methodology, Investigation, Validation, Supervision, Formal analysis, Visualization, Writing – original draft.

Cristina Pablos: Formal analysis, Resources, Supervision, Writing – review & editing. **Patricia Misis:** Investigation, Formal analysis, Writing – review & editing. **Sandra Pascua:** Investigation, Formal analysis, Writing – review & editing. **Javier Marugán:** Conceptualization, Methodology, Formal analysis, Resources, Supervision, Writing – review & editing, Funding acquisition.

Data availability

Data will be made available on request.

Declaration of competing interest

The authors declare that they have no known competing financial interests or personal relationships that could have appeared to influence the work reported in this paper.

Acknowledgements

The authors gratefully acknowledge the financial support of the Spanish State Research Agency (AEI) and the Spanish Ministry of Science and Innovation through the project AQUAENAGRI (PID2021-126400OB-C32) and Comunidad de Madrid through the program REMTAVARES (P2018/EMT-4341).

References

Adán, C., Marugán, J., Sánchez, E., Pablos, C., Van Grieken, R., 2016. Understanding the effect of morphology on the photocatalytic activity of TiO2 nanotube array electrodes. Electrochim. Acta 191, 521–529. https://doi.org/10.1016/j.electacta.2016.01.088.

APHA (American Public Health Association), 2012. Standard Methods for the Examination of Water and Wastewater. Stand. Methods Exam. Water Wastewater. p. 1496.

Balaji, S., Djaoued, Y., Robichaud, J., 2006. Phonon confinement studies in nanocrystalline anatase-TiO2 thin films by micro Raman spectroscopy. J. Raman Spectrosc. 37, 1416–1422. https://doi.org/10.1002/jrs.1566.

Brillas, E., Martínez-Huitle, C.A., 2015. Decontamination of wastewaters containing synthetic organic dyes by electrochemical methods. An updated review. Appl. Catal. B Environ. 166–167, 603–643. https://doi.org/10.1016/j.apcatb.2014.11.016.

Cheng, X. Fang, Leng, W. Hua, Pi, O. Yang, Zhang, Z., Zhang, J. Qing, Cao, C. Nan, 2007. Enhancement of photocatalytic activity of TiO2 film electrode by in situ photoelectro-generating active chlorine. Trans. Nonferrous Met. Soc. China (English Ed) 17, 1087–1092. https://doi.org/10.1016/S1003-6326(07)60230-1.

Chi, Y., Xu, S., Li, M., He, M., Yu, H., Li, L., Yue, Q., Gao, B., 2020. Effective blockage of chloride ion quenching and chlorinated by-product generation in photocatalytic wastewater treatment. J. Hazard. Mater. 396. https://doi.org/10.1016/j.jhazmat.2020.122670.

Chung, C.M., Hong, S.W., Cho, K., Hoffmann, M.R., 2018. Degradation of organic compounds in wastewater matrix by electrochemically generated reactive chlorine species: kinetics and selectivity. Catal. Today 313, 189–195. https://doi.org/10.1016/j.cattod.2017.10.027.

Day, S., Lalitha, P., Haug, S., Fothergill, A.W., Cevallos, V., Vijayakumar, R., Prajna, N.V., Acharya, N.R., McLeod, S.D., L, T.M., 2009. Activity of antibiotics against Fusarium and Aspergillus. Br. J. Ophthalmol. 93, 116–119. https://doi.org/10.1136/bjo.2008.142364.

Ersoy, Z.G., Dinc, O., Cinar, B., Gedik, S.T., Dimoglo, A., 2019. Comparative evaluation of disinfection mechanism of sodium hypochlorite, chlorine dioxide and electroactivated water on Enterococcus faecalis. Lwt 102, 205–213. https://doi.org/10.1016/j.lwt.2018.12.041.

Fraga, L.E., Anderson, M.A., Beatriz, M.L.P.M.A., Paschoal, F.M.M., Romão, L.P., Zanoni, M.V.B., 2009. Evaluation of the photoelectrocatalytic method for oxidizing chloride and simultaneous removal of microcystin toxins in surface waters. Electrochim. Acta 54, 2069–2076. https://doi.org/10.1016/j.electacta.2008.08.060.

García-Espinoza, J.D., Robles, I., Durán-Moreno, A., Godínez, L.A., 2021. Photo-assisted electrochemical advanced oxidation processes for the disinfection of aqueous solutions: a review. Chemosphere 274. https://doi.org/10.1016/j.chemosphere.2021.129957.

Gong, J., Lai, Y., Lin, C., 2010. Electrochemically multi-anodized TiO2 nanotube arrays for enhancing hydrogen generation by photoelectrocatalytic water splitting. Electrochim. Acta 55, 4776–4782. https://doi.org/10.1016/j.electacta.2010.03.055.

Hoff, J.C., Akin, E.W., 1986. Microbial resistance to disinfectants: mechanisms and significance. Environ. Health Perspect. 69, 7–13. https://doi.org/10.1289/ehp.86697.

Huang, X., Qu, Y., Cid, C.A., Finke, C., Hoffmann, M.R., Lim, K., Jiang, S.C., 2016. Electrochemical disinfection of toilet wastewater using wastewater electrolysis cell. Water Res. 92, 164–172. https://doi.org/10.1016/j.watres.2016.01.040.

Jeong, J., Kim, C., Yoon, J., 2009. The effect of electrode material on the generation of oxidants and microbial inactivation in the electrochemical disinfection processes. Water Res. 43, 895–901. https://doi.org/10.1016/j.watres.2008.11.033.

Junli, H., Li, W., Nenqi, R., Li, L.X., Fun, S.R., Guanle, Y., 1997. Disinfection effect of chlorine dioxide on viruses, algae and animal planktons in water. Water Res. 31, 455–460. https://doi.org/10.1016/S0043-1354(96)00276-X.

Kalantar-zadeh, K., Sadek, A.Z., Partridge, J.G., McCulloch, D.G., Li, Y.X., Yu, X.F., Spizzirri, P.G., Wlodarski, W., 2009. Nanoporous titanium oxide synthesized from anodized filtered cathodic vacuum arc Ti thin films. Thin Solid Films 518, 1180–1184. https://doi.org/10.1016/j.tsf.2009.03.223.

Kim, J., Kim, C., Kim, S., Yoon, J., 2018. RuO2 coated blue TiO2 nanotube array (blue TNA-RuO2) as an effective anode material in electrochemical chlorine generation. J. Ind. Eng. Chem. 66, 478–483. https://doi.org/10.1016/j.jiec.2018.06.015.

Kraft, A., Stadelmann, M., Blaschke, M., Kreysig, D., Sandt, B., Schro, F., Rennau, J., 1999. Electrochemical water disinfection part I: hypochlorite production from very dilute chloride solutions. J. Appl. Electrochem. 29, 861–868.

Le Luu, T., Kim, J., Yoon, J., 2015. Physicochemical properties of RuO2 and IrO2 electrodes affecting chlorine evolutions. J. Ind. Eng. Chem. 21, 400–404. https://doi.org/10.1016/j.jiec.2014.02.052.

Li, G., Liu, X., Zhang, H., An, T., Zhang, S., Carroll, A.R., Zhao, H., 2011. In situ photoelectrocatalytic generation of bactericide for instant inactivation and rapid decomposition of Gram-negative bacteria. J. Catal. 277, 88–94. https://doi.org/10.1016/j.jcat.2010.10.011.

Li, G., Liu, X., Zhang, H., Wong, P.K., An, T., Zhao, H., 2013. Comparative studies of photocatalytic and photoelectrocatalytic inactivation of E. coli in presence of halides. Appl. Catal. B Environ. 140–141, 225–232. https://doi.org/10.1016/j.apcatb.2013.04.004.

Marugán, J., van Grieken, R., Pablos, C., Sordo, C., 2010. Analogies and differences between photocatalytic oxidation of chemicals and photocatalytic inactivation of microorganisms. Water Res. 44, 789–796. https://doi.org/10.1016/j.watres.2009.10.022.

Mesones, S., Mena, E., López Muñoz, M.J., Adán, C., Marugán, J., 2020. Synergistic and antagonistic effects in the photoelectrocatalytic disinfection of water with TiO2 supported on activated carbon as a bipolar electrode in a novel 3D photoelectrochemical reactor. Sep. Purif. Technol. 247, 117002. https://doi.org/10.1016/j.seppur.2020.117002.

Nash, T., 1953. The colorimetric estimation of formaldehyde by means of the Hantzsch reaction. Biochem. J. 55, 416–421. https://doi.org/10.1042/bj0550416.

O Young, R., 2016. Chlorine dioxide (CLO2) as a non-toxic antimicrobial agent for virus, bacteria and yeast (Candida albicans). Int. J. Vaccine Res. 2, 1–12. https://doi.org/10.15406/ijvv.2016.02.00052.

Oliveira, F.H., Osugi, M.E., Paschoal, F.M.M., Profeti, D., Olivi, P., Zanoni, M.V.B., 2007. Electrochemical oxidation of an acid dye by active chlorine generated using Ti/Sn(1-x)Ir x O2 electrodes. J. Appl. Electrochem. 37, 583–592. https://doi.org/10.1007/s10800-006-9289-6.

Pablos, C., Marugán, J., Van Grieken, R., Adán, C., Riquelme, A., Palma, J., 2014. Correlation between photoelectrochemical behaviour and photoelectrocatalytic activity and scaling-up of P25-TiO2 electrodes. Electrochim. Acta 130, 261–270. https://doi.org/10.1016/j.electacta.2014.03.038.

Pulgarin, C., Kiwi, J., Nadtochenko, V., 2012. Mechanism of photocatalytic bacterial inactivation on TiO2 films involving cell-wall damage and lysis. Appl. Catal. B Environ. 128, 179–183. https://doi.org/10.1016/j.apcatb.2012.01.036.

Sales Monteiro, M.K., Sales Monteiro, M.M., de Melo Henrique, A.M., Llanos, J., Saez, C., Dos Santos, E.V., Rodrigo, M.A., 2021. A review on the electrochemical production of chlorine dioxide from chlorates and hydrogen peroxide. Curr. Opin. Electrochem. 27, 100685. https://doi.org/10.1016/j.coelec.2020.100685.

Saygin, H., Baysal, A., 2022. Influence of Ca species on the surface properties of TiO2 nanoparticles and its possible transformation. Bull. Mater. Sci. 45. https://doi.org/10.1007/s12034-022-02735-z.

Scialdone, O., Proietto, F., Galia, A., 2021. Electrochemical production and use of chlorinated oxidants for the treatment of wastewater contaminated by organic pollutants and disinfection. Curr. Opin. Electrochem. 27, 100682. https://doi.org/10.1016/j.coelec.2020.100682.

Selcuk, H., Anderson, M.A., 2005. Effect of pH, charge separation and oxygen concentration in photoelectrocatalytic systems: active chlorine production and chlorate formation. Desalination 176, 219–227. https://doi.org/10.1016/j.desal.2004.10.016.

Sirés, I., Brillas, E., Oturan, M.A., Rodrigo, M.A., Panizza, M., 2014. Electrochemical advanced oxidation processes: today and tomorrow. A review. Environ. Sci. Pollut. Res. 21, 8336–8367. https://doi.org/10.1007/s11356-014-2783-1.

Sisti, M., Brandi, G., De Santi, M., Rinaldi, L., Schiavano, G.F., 2012. Disinfection efficacy of chlorine and peracetic acid alone or in combination against Aspergillus spp. and Candida albicans in drinking water. J. Water Health 10, 11–19. https://doi.org/10.2166/wh.2011.150.

van Grieken, R., Marugán, J., Pablos, C., Furones, L., López, A., 2010. Comparison between the photocatalytic inactivation of Gram-positive E. faecalis and Gram-negative E. coli faecal contamination indicator microorganisms. Appl. Catal. B Environ. 100, 212–220. https://doi.org/10.1016/j.apcatb.2010.07.034.

Vijayakumar, R., Sandle, T., 2019. A review on biocide reduced susceptibility due to plasmid-borne antiseptic-resistant genes—special notes on pharmaceutical environmental isolates. J. Appl. Microbiol. 126, 1011–1022. https://doi.org/10.1111/jam.14118.

Xiao, S., Wan, D., Zhang, K., Qu, H., Peng, J., 2016. Enhanced photoelectrocatalytic degradation of ammonia by in situ photoelectrogenerated active chlorine on TiO2 nanotube electrodes. J. Environ. Sci. (China) 50, 103–108. https://doi.org/10.1016/j.jes.2016.04.028.

Xiao, K., Zhou, B., Chen, S., Yang, B., Zhang, J., Zhu, C., 2019. Enhanced photoelectrocatalytic breakdown of Cu-cyanide complexes and copper recovery using photoelectrogenerated free chlorine. Electrochem. Commun. 100, 34–38. https://doi.org/10.1016/j.elecom.2019.01.018.

Zanoni, M.V.B., Sene, J.J., Selcuk, H., Anderson, M.A., 2004. Photoelectrocatalytic production of active chlorine on nanocrystalline titanium dioxide thin-film electrodes. Environ. Sci. Technol. 38, 3203–3208. https://doi.org/10.1021/es0347080.

Zhang, W., An, T., Cui, M., Sheng, G., Fu, J., 2005. Effects of anions on the photocatalytic and photoelectrocatalytic degradation of reactive dye in a packed-bed reactor. J. Chem. Technol. Biotechnol. 80, 223–229. https://doi.org/10.1002/jctb.1185.

Zhao, Y., Fan, Q., Wang, X., Zhang, W., Hu, X., Liu, C., Liang, W., 2019. Photoelectrocatalytic degradation of microcystin-LR using a dimensionally stable anode and the assessment of detoxification. Chem. Eng. J. 368, 968–979. https://doi.org/10.1016/j.cej.2019.03.029.